

Assessing the surface downward longwave irradiance models using ERA5 input data in Canada



Mostafa Khorsandi,^{a,b} Andre St-Hilaire,^{a,b} Richard Arsenault,^c

^a *Institut National de la Recherche Scientifique, Centre Eau Terre Environnement (INRS-ETE), 490 De la Couronne St., Quebec City, Quebec, G1K 9A9, Canada (mostafa.khorsandi@inrs.ca)*

^b *Canadian Rivers Institute, UNB Fredericton, 28 Dineen Dr Fredericton, New Brunswick, E3B 5A3, Canada (andre.st-hilaire@inrs.ca)*

^c *Hydrology, climate and climate change laboratory, École de technologie supérieure (ÉTS), Montréal, Quebec, Canada (richard.arsenault@etsmtl.ca)*

Corresponding author: Mostafa Khorsandi, mostafa.khorsandi@inrs.ca

ABSTRACT

Longwave radiation (LR) is one of the energy balance components responsible for warming and cooling water during hot summers. Both downward incoming LR, emitted by the atmosphere, and outgoing LR emitted by land surface are not widely measured. The influence of clouds on the LR heat budget makes it even harder to establish reliable formulations for all-sky conditions. This paper uses air temperature and cloud cover from the ERA5 reanalysis database to compare 20 models for the downward longwave irradiance (DLI) at the Earth's surface and compare them with ERA5's DLI product. Our work uses long-time continuous DLI measured data at three stations over Canada, and ERA5 reanalysis, a reliable source for data-scarce regions, such as central British Columbia (Canada). The results show the feasibility of the local calibration of different formulations using ERA5 reanalysis data for all-sky conditions with RMSE metrics ranging from 37.1 to $267.3 \frac{W}{m^2}$, which is comparable with ERA5 reanalysis data and can easily be applied at broader scales by implementing it into hydrological models. Moreover, it is shown that ERA5 gridded data for DLI shows the best results with RMSE = $31.7 \frac{W}{m^2}$. This higher performance suggests using ERA5 data directly as input data for hydrological and ecological models.

Key Words: Long Wave Radiation, ERA5 data, Empirical Models.

1. Introduction

Longwave radiation (LR) is one of the main heat budget terms responsible for multiple environmental processes in land and aquatic environments (Bernhardt et al. 2022; McFarlane; Clark 2021; Ouellet et al. 2014). LR exchange, which usually refers to wavelengths longer than four μm from rivers, is controlled by the surface's thermal emissivity, atmospheric objects, clouds, water vapor, and carbon dioxide (Herrero; Polo 2012). There are two LR-related variables (downward and upward radiation); the downward longwave irradiance (DLI) acts as a signature of the atmosphere condition (Tang et al. 2021). Therefore, it controls an important part of the surface heat budget (Zhou et al. 2020). One of the critical roles of LR is cooling water during summer, which significantly impacts aquatic flora and fauna. A previous study has shown that this component of the heat budget balance is responsible for cooling the water temperature in the Nechako watershed in central British Columbia, Canada (Khorsandi et al., 2022). Therefore, using a more accurate longwave radiation balance in this region for energy balance modeling is necessary. The more precise representation of DLI can improve the

simulation results and analysis of hydrological and water quality (e.g., temperature) models (Gatien et al. 2022; Khorsandi et al. 2022).

Over the past decades, multiple studies developed the scientific foundations for DLI (Zhou et al. 2020). Although the physical foundation for DLI is well understood and represented based on Stephan-Boltzman law, the knowledge related to the interaction of variables that affect atmospheric emissivity is still developing. As a result, multiple studies parameterized and studied DLI using several equations (Bárbaro et al. 2009; Duarte et al. 2006; Herrero; Polo 2012; Huang et al. 2007; Koll; Cronin 2018; Sicart et al. 2010). Idso; Jackson (1969) developed a general formula for the surface DLI estimation using theoretical analysis of atmospheric thermal behavior. Using global scale measurements, they found that DLI has the minimum effective emittance at 273K. Based on this finding, they presented a new equation for ground surface DLI modeling.

Multiple studies improved the work by Idso; Jackson (1969), which Miller (1981) compiled for the energetics of ecosystems (Miller 1981). His textbook presented formulations and applications of DLI for ecosystem modeling. Afterward, multiple scholars developed formulations mainly for air emissivity. It is well known that cloud cover is the primary controlling meteorological variable with impacts on DLI through emissivity after air temperature (Li et al. 2017; Zhou et al. 2020).

With the advances in data acquisition, cloud cover impact has been studied significantly. Duarte et al. (2006) studied the clear sky and cloudy sky DLI using well-known parameterizations in Southern Brazil; Sicart et al. (2010) did the same for Andean glaciers, Herrero; Polo (2012) for a mountainous site, and Voortman et al. (2015) for dune ecosystems. These studies have shown the efficiency of already developed models in providing reliable estimates in cloudy-sky conditions.

More recent studies paid greater attention to all sky parameterizations (Li et al. 2017; Long et al. 2021). For example, Li et al. (2017) compared and recalibrated fifteen parametric models for DLI. They showed that previously proposed DLI models can be categorized into only a few families of models. They recommended the Brunt (Brunt 1932) family of models for future use. Long et al. (2021) tested six models for clear-sky conditions and eight for cloudy conditions over the Tibetan Plateau. Their results showed an average of 26.4 W/m² for RMSE as the efficiency metric for all-sky conditions. The analysis of cloud cover impact on DLI converged to the intercomparison with reanalysis data. Tang et al. (2021) showed that

reanalysis products for DLI outperform satellite retrievals over the land surface. They pointed out the extensive possibility of reanalysis usage for DLI modeling.

Parallel to the cloud impact assessments and development on DLI, the impact of other meteorological variables has been studied via clear sky conditions. Prata (1996) focused on clear sky conditions and developed his equation. He formulated his equation based on the impact of air temperature and water vapor on DLI. Multiple studies showed vapor pressure as the second primary controlling variable on air emissivity (Abramowitz et al. 2012; Dilley; O'brien 1998; Huang et al. 2007; Li et al. 2017; Morcrette 2002; Niemelä et al. 2001; Zhou; Cess 2000).

It can be seen that DLI is well formulated, and the main controllers of DLI emissivity are air temperature, cloud cover, and water vapor pressure. Also, the usage of reanalysis data as a proxy for meteorological variables was recommended in the literature (Gatien et al. 2022; Tarek et al. 2020). However, there is no previous research for data-scarce regions that can benefit from reanalysis data as a proxy for meteorological measurements to calculate DLI or the reanalysis-based product for DLI.

This work presents a comparative analysis of different DLI formulations using the 2 Dec 2019 to 31 May 2022 period of hourly observation of DLI with hourly ERA5 reanalysis meteorological data. The study area is the Nechako watershed (British Columbia, Canada), which has two stations to measure DLI [at Skins Lake spillway (SLS) and Kenny dam, see Fig. 1]. Using this analysis, locally selected parameterizations for emissivity for all-sky conditions, based on hourly ERA5 data, are proposed, calibrated using measurements at SLS, and validated against measurements at Kenny dam, 75km from SLS. The significance of the results using the second validation station on an experimental drainage basin operated by the *École de Technologie Supérieure* (QC, Canada) is called the 'BVE Sainte-Marthe Station' (hereafter BVE station). Two different approaches were performed and validated at the study site for DLI modeling: (1) comparing the physically-based parameterizations of previous equations in the literature and (2) using ERA5 gridded DLI data instead of calculating DLI. Finally, the possible application of the different parameterizations developed are addressed for future modeling at the Nechako watershed.

2. Materials and Methods

a. Study area

The Nechako River watershed has a 45,000 km² drainage area with two main rivers, Nechako and Nautley. This watershed is located in the central part of British Columbia, Canada (Fig. 1). The present paper focuses on the two aforementioned measuring sites for radiation measurements: SLS and Kenny Dam (Table 1). These two stations are located on the shore along the Kenny Dam Reservoir, with low canopy cover (Fig. A1 in Appendix A). The observed data were used without any pre-processing.

Table 1: The names and locations of longwave radiation measuring stations

Station	Longitude (West)	Latitude (North)	Elevation (masl)	Distance from closest ERA5 grid point (Km)	Data availability	
					Start	End
Skins Lake Spillway	-125.997	53.77	865	2.5	2 Dec 2019	31 May 2022
Kenny Dam BVE	-124.95 -74.28	53.58 45.43	857 144	9.7 12.2	2 Dec 2019 1 Nov 2018	31 May 2022 31 Oct 2022

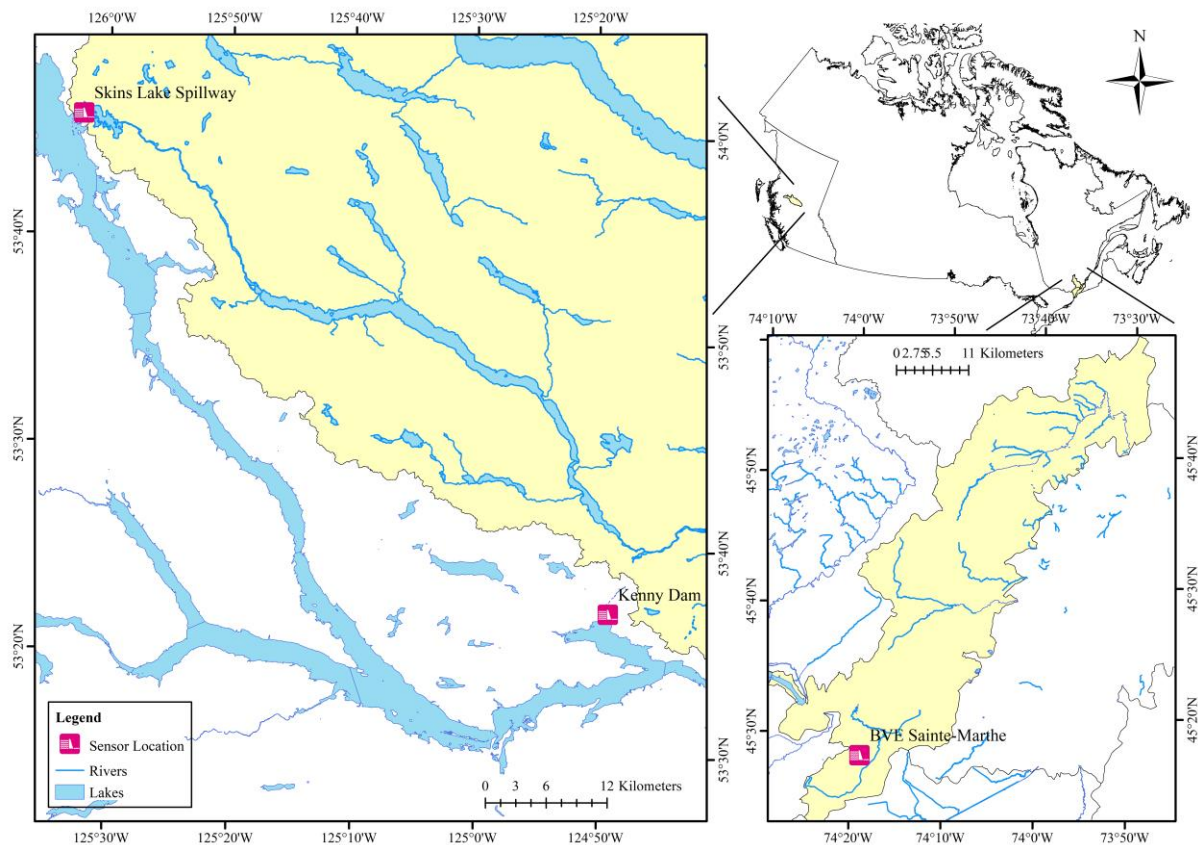


Fig. 1. Nechako River and BVE Sainte-Marthe watersheds and measuring stations, SLS, Kenny Dam, and BVE

The SLS station was used for calibration and the Kenny Dam station for validation. The third station which was used for validation was the BVE station (<http://bvesm.etsmtl.ca/>) (Fig. 1 and Table 1). This station is located approximately 70 km west of Montreal in Quebec, Canada (45.43N, 74.28W). Among all the measured hydroclimate variables, DLI was used. In contrast to the other stations, the BVE station is located in an area with a dense canopy (Fig. A1 in Appendix A). The observed data showed a persistent bias compared to ERA5 data and all DLI calculation models. This bias (Equation 26 in Section 2f) was calculated using the simulated and observed values. Therefore, as the pre-processing for this station, the bias was calculated and subtracted from the measured values.

b. ERA5 reanalysis data

The required input meteorological variables for the models were provided by the European Center for Medium-Range Weather Forecasting (ECMWF) through their European Reanalysis 5th generation (ERA5) (Hersbach et al. 2020). ERA5 reanalysis data cover all required meteorological variables. Gatien et al. (2022) showed the possibility of using ERA5 reanalysis data for water temperature modeling in calibration and simulation steps using the Nechako River as their case study. In this study, three variables from the ERA5 database were used: (1) DLI (W/m^2), (2) air temperature at 2 m height ($^{\circ}C$), and (3) total cloud cover (Dimensionless). The 2 m height data were used based on common meteorological standards and the DLI sensors installed at the same height. ERA5 gridded-based data were used hourly from the closest grid points to our measuring stations.

c. Longwave heat budget modeling

The most fundamental equation for longwave radiation is the Stefan-Boltzmann Equation. The Stefan–Boltzmann law is a well-known equation to quantify the power radiated from a black body in terms of its temperature. It expresses that the total energy emitted from a black body object per unit area per time is proportional to the fourth power of black body temperature in Kelvin:

$$J = \sigma T^4 \quad (1)$$

where J = radiant emittance (Wm^{-2}), σ = Stefan–Boltzmann constant ($5.670373 \times 10^{-8} Wm^{-2}K^{-4}$), and T = thermodynamic temperature (K). Not all radiation is re-emitted for natural objects, like a perfect black body, and the emissivity varies with wavelength. However,

the total emissivity for natural objects is usually estimated using a constant without considering wavelength dependency. The final equation is:

$$J = \beta \sigma T^4 \quad (2)$$

where β = emissivity of the object ($0 < \beta < 1$). This equation can be used as downward incoming longwave radiation for clear sky conditions. To estimate air emissivity (β), some equations are proposed for hydrological studies. For example, Morin; Couillard (1990) presented the following equation:

$$\beta = (0.74 + 0.0065e_a)(1 + 0.17B^2) \quad (3)$$

where e_a = vapor pressure (*mm Hg*) and B = total cloud cover (*dimensionless*). Among all cloud related variables, total cloud cover is usually used for applied studies (Morin; Couillard 1990; Morin et al. 1994; Ouellet et al. 2014). For west Canada, Gatien et al. (2022) showed the usage efficiency of total cloud cover to calculate total heat budget impacting water temperature. However, different clouds with completely different effects on DLI can have the same total cloud cover value (e.g., Cirrus clouds may have higher efficiency than low-level stratiform clouds in influencing DLI, while cirrus cloud and low-level stratiform clouds or the combination of them can give the same value of total cloud cover). As it is often done in other studies, there is no discrimination done for different types of clouds in the present study. The DLI equations consider the longwave heat from the atmosphere as a 1D phenomenon instead of 3D. Also, the variables used in these equations are close to the surface measurements and developed based on the total cloud cover variable. Therefore, the most probable choice from the ERA5 dataset to implement in this study is to use the total cloud cover variable. Alternatively to calculated β , Fassnacht (2001) mentioned the following equation:

$$\beta = (0.53 + 0.2055e_a^{0.5})(1 + 0.40B) \quad (4)$$

e_a can be estimated using Tetens equations and T_{air} as follows:

$$e_a = 7.50062 \times \begin{cases} 0.061078 \times \exp\left(\frac{17.27T_{air}}{T_{air} + 237.3}\right), & T_{air} \geq 0^\circ C \\ 0.061078 \times \exp\left(\frac{21.875T_{air}}{T_{air} + 265.5}\right), & T_{air} < 0^\circ C \end{cases} \quad (5)$$

It has been shown that cloud cover and vapor pressure significantly impact the incoming longwave radiation from the air (Hogan; Bozzo 2016; Morcrette 2002; Schafer 2017). However, the relationship between effective emissivity for a cloudy condition related to cloud

cover, air temperature, and vapor pressure is complicated. One method is to use advanced global climate models output products, empowered with computational fluid dynamic methods, to tackle the complex relationship of thermodynamic variables. These models and their products are the utmost recent developments for DLI calculations in atmospheric science. However, historically, simple mathematical formulations have been used to calculate DLI for local and terrestrial purposes. Sugita; Brutsaert (1993) studied the impact of cloud effect on downward longwave radiation. They categorized equations for two conditions: (1) clear sky and (2) cloudy sky, as described below.

1) CLEAR SKY LONGWAVE RADIATION

Sugita; Brutsaert (1993) showed that equation (2) is accurate enough for a clear sky. The only problem is estimating β . They reviewed different equations to estimate β as follows:

$$\beta = 1 - a_1 \exp[b_1(273 - T_{air})^2] \quad (\text{Idso; Jackson 1969}) \quad (6)$$

$$\beta = a_2 \left(\frac{e_a}{T_{air}}\right)^{b_2} \quad (\text{Brutsaert 1975}) \quad (7)$$

$$\beta = a_3 [1 - \exp(-e_a \frac{T_{air}}{b_3})] \quad (\text{Satterlund 1979}) \quad (8)$$

$$\beta = a_4 + b_4 e_a^{0.5} \quad (\text{Sellers 1965}) \quad (9)$$

where: a_x, b_x, c_x ($x = 1 \dots 4$) are constants that need to be calibrated.

Since T_{air} and e_a are essential parameters to estimate β for clear sky, Huang et al. (2007) studied clear-sky outgoing longwave radiation sensitivity to these variables. Their results showed that T_{air} has a dominant impact compared to e_a in the low or middle troposphere, while in the upper troposphere, the impacts of each component are nearly equal. In this study T_{air} and e_a refer to 2-meter measurements.

Some authors prefer to estimate longwave radiation heat flux for clear sky based on equations other than Stephan-Boltzman. They proposed several equations, which Ouellet et al. (2014) listed as follows:

$$J_{air} = J_{a_0} + \sigma(T_{air}^4 - J_{a_0})B^{1.4}\alpha \quad (\text{Ouellet et al. 2014}) \quad (10)$$

with $J_{a_0} = 1 - 0.261 \exp(-0.000777T_{air}^2)$

$$J_{air} = \beta \sigma T_{air}^4 B^{-0.0227} \alpha \quad (\text{Surgita and Brutsaert 1993}) \quad (11)$$

$$J_{air} = 5.16453 \times 10^{-13} [1 + (0.17B^2)] T_{air}^6 \quad (\text{Lai; Mooney 2009}) \quad (12)$$

where α = empirical coefficient (dimensionless).

Barbaro et al. (2010) concluded that because the previous equations do not contain enough information about the daily vertical dynamics of air temperature and water vapor, they possibly fail to model the surface emissivity's daily variation. They, therefore, suggested a more accurate way to estimate J_{air} for clear-sky conditions using an expression derived from a purely empirical approach. Barbaro et al. (2010) used 5 min averaged time series for longwave radiation to develop an experimental equation. This time step can capture most longwave patterns, e.g., hourly, daily, and monthly variabilities. Their equation predicts better values than previous equations in the literature for clear sky conditions in Sau Paulo. This equation was:

$$J_{air} = 1827.231 + 31.35T_{air} - 35.06e_a - 967.82 \ln T_{air} - \frac{7725.26}{T_{air}} + 390.92\sqrt{e_a} + \frac{2372.20}{e_a} \quad (13)$$

where e_a (hPa). They also mentioned some other experimental equations for clear sky conditions suggested before them as follows:

$$J_{air} = (0.52 + 0.065\sqrt{e_a})\sigma T_{air}^4 \quad (\text{Brunt 1932}) \quad (14)$$

$$J_{air} = (9.2 \times 10^{-6} T_{air}^2)\sigma T_{air}^4 \quad (\text{Swinbank 1963}) \quad (15)$$

$$J_{air} = (1 - [1 + 46.5 \left(\frac{e_a}{T_{air}}\right)] \exp \left\{ - \left[1.2 + 3 \left[46.5 \left(\frac{e_a}{T_{air}}\right) \right]^{1/2} \right] \right\}) \sigma T_{air}^4 \quad (16)$$

(Prata 1996)

$$J_{air} = 59.38 + 113.7 \left(\frac{T_{air}}{273.16}\right)^6 + 96.96 \sqrt{18.6 \left(\frac{e_a}{T_{air}}\right)} \quad (\text{Dilley; O'brien 1998}) \quad (17)$$

$$J_{air} = \begin{cases} [0.72 + 0.009(e_a - 1.5)]\sigma T_{air}^4, & e_a \geq 1.5 \\ [0.72 - 0.076(e_a - 1.5)]\sigma T_{air}^4, & e_a < 1.5 \end{cases} \quad (\text{Niemelä et al. 2001}) \quad (18)$$

2) CLOUDY SKY LONGWAVE RADIATION

Clouds trap longwave radiation and can re-emit it, thereby increasing the amount of radiation reaching the surface. Therefore, DLI equations should include cloud cover for practical purposes (Duarte et al. 2006). Although cloud cover and cloud parameters are measured by satellite imagery, ground-based measurements are not always available. The cloudy sky condition is easily observable, nevertheless hard to quantify. The complexity of measuring cloud cover is due to its relatively small scale size, the height of clouds, the cloud formation, and types, and the prohibitive cost of measurement devices. Although cloud cover is monitored in crucial places like airports, their data are for local purposes and not easily transferable to larger regions. When cloud cover measurements are unavailable, they can be estimated by Crawford and Duchon equation (Crawford; Duchon 1999). However, this equation can only be used for daytime when downward solar radiation measurements are available (Choi et al. 2008). There are two possible alternative methods of estimation for all sky conditions:

First, it is possible to use reanalysis products for cloud cover. The assimilated products of reanalysis climate models provide a reasonably acceptable estimation for cloud cover for large-scale studies (Gatien et al. 2022; Tang et al. 2021; Yao et al. 2019; Yao et al. 2020). However, different cloud types have a distinct influence on DLI. Since different cloud types can be active simultaneously and influence DLI, the total cloud cover is used. Cloud cover is one of the most uncertain variables among reanalysis products since it's purely influenced by the implemented atmospheric models and is model-dependent (Free et al. 2016; Yao et al. 2019; Yao et al. 2020). Among all the cloud properties, the total cloud cover is most measurable using satellite imagery incorporated in reanalysis models. Therefore, the reanalysis of assimilated products is more reliable for this variable. Also, it is an aggregate indicator of all clouds in the sky. Yao et al. (2019) compared three reanalysis products for East Asia and concluded that they could represent the cloud characteristics. Their results showed that CRA reanalysis better represents the total cloud cover than the other two reanalysis datasets (ERA5 and MERRA2) for East Asia. To our knowledge, Canada has no previous study to compare reanalysis products with the measurements for cloud cover variables. However, multiple case studies using ERA5 showed this reanalysis product's suitability for different hydrological cycle processes (Gatien et al. 2022; Khorsandi et al. 2022; Tarek et al. 2020). Total cloud cover is the widespread cloud-related measurement in Canada, mainly measured in airports (Milewska 2004). Moreover, Canada has stopped producing synoptic cloud cover reports due to the Automated Weather Observing Systems (AWOS) since 1990 (Milewska 2004). Although specific sensors are

designed to measure the cloud cover parameters (www.atmos-meteo.com), to our knowledge, there are no measurements for such sensors in the Nechako watershed, and cloud-related studies are among the least studied subjects in Canada (Milewska 2004). Therefore, the second method uses the reanalysis of cloud cover data for cloudy conditions. A typical approach is to adjust $J_{clear\ sky}$ using correction factor equations (e.g., Bolz (1949) or Budyko (1974)) as follows:

$$J_{cloudy\ sky} = J_{clear\ sky}(1 + uB^v) \quad (19)$$

where u and v are constants with different values in each reference. Bolz (1949) used $v = 2$ for different values of u . Some examples of this form presented by other scholars (Duarte et al. 2006) for various case studies where $-1 \leq u \leq 1$ and $0 \leq v \leq 4$.

d. ECMWF radiation scheme ERA5 data and DLI

Hogan; Bozzo (2016) presented the calculation scheme within the ECMWF model [Integrated Forecasting System (IFS)], which is the “Longwave layer-wise emission” scheme to calculate multiple atmospheric variables, including DLI. The formulation can be shown as the following equation:

$$\frac{dH_{long\downarrow}}{d\delta} = D(-H_{long\downarrow} + F_{i-\frac{1}{2}} + \delta F') \quad (20)$$

where $D = 1.66$ is the diffusivity factor accounting for longwave heat transport, $F_{i-\frac{1}{2}}$ is the Planck function above i^{th} atmosphere layer, and F' is the gradient of the Planck function (Hogan; Bozzo 2016). This three-dimensional (each calculation cell is based on longitude, latitude, and altitude differentiation) modeling of DLI by the ECMWF atmosphere model uses thermodynamic laws for the atmosphere system, which cannot be compared with one-dimensional modeling approaches. However, the result of this model needs to be assessed for inland data-scarce regions for future implementations.

e. Calibration algorithm

The calibration algorithm is the Covariance Matrix Adaptation Evolution Strategy (CMA-ES), an evolutionary algorithm developed by (Hansen 2016). CMA-ES is a global optimization method able to solve high-dimensional problems. These benefits make it a good candidate as a general-purpose optimization method (Hansen; Ostermeier 1996). This algorithm is assessed

as a superior candidate for use in hydrology (Arsenault et al. 2014). CMA-ES follows four steps until a stopping criterion is met, fully explained by Hansen (2016). The only stopping criterion used is the number of evaluations (10000). The lower and upper boundaries for calibration variables were defined based on the literature recommendations.

f. Calibration of coefficients in DLI equations

This study used the Root Mean Square Error (*RMSE*) as the objective function for all calibrations, aiming to find the optimal values for each model’s coefficients. *RMSE* was used to calibrate the model parameters since it is one of the general efficiency metrics often used to measure the performance of temperature models by focusing on all data without focusing on a specific part of the data (e.g., high values or low values) (Gupta et al. 2009; Legates; McCabe Jr 1999). At the same time, it is shown that none of the efficiency criteria perform ideally to show the goodness of fit (Krause et al. 2005). Therefore, multiple efficiency metrics were calculated as strongly recommended by Legates; McCabe Jr (1999), as well as Gauch et al. (2022).

Relative Root Mean Square Error (*RRMSE*) was used to show each equation’s skill in a dimensionless way both for calibration and validation steps. Nash–Sutcliffe efficiency (*NSE*) shows a statistically meaningful efficiency of fit as well as the performance of fit for high values. The correlation (*r*) and coefficient of determination (*R*²) metrics were presented as recommended by Legates; McCabe Jr (1999). Since using more parameters and input variables can cause overfitting, there is a need to help for choosing better models while keeping the models parsimonious. To this goal, the Akaike information criterion (*AIC*) (Akaike 1974) and Bayesian information criterion (*BIC*) (Schwarz 1978) were also calculated to help select the best models while considering the number of parameters. Finally, a simple bias metric was calculated to show the level of bias between simulations and observed data.

A summary of these metrics is presented as follows:

$$RMSE_j = \sqrt{\frac{\sum_{i=1}^N (S_{i,j} - O_{i,j})^2}{N}} \quad (21)$$

$$RRMSE_j = \frac{RMSE_j}{\bar{O}_j} \times 100 \quad (22)$$

$$r_j = \frac{\sum_{i=1}^N (S_{i,j} - \bar{S}_j)(O_{i,j} - \bar{O}_j)}{\sqrt{\sum_{i=1}^N (S_{i,j} - \bar{S}_j)^2 \sum_{i=1}^N (O_{i,j} - \bar{O}_j)^2}} \quad (23)$$

$$R_j^2 = \frac{\sum_{i=1}^N (S_{i,j} - \bar{S}_j)(O_{i,j} - \bar{O}_j)}{[\sqrt{\sum_{i=1}^N (S_{i,j} - \bar{S}_j)^2 \sum_{i=1}^N (O_{i,j} - \bar{O}_j)^2}]^2} \quad (24)$$

$$NSE_j = 1 - \frac{\sum_{i=1}^N (S_{i,j} - O_{i,j})^2}{\sum_{i=1}^N (O_{i,j} - \bar{O}_j)^2} \quad (25)$$

$$Bias_j = \bar{O}_j - \bar{S}_j \quad (26)$$

$$AIC_j = N \cdot \ln\left(\frac{\sum_{i=1}^N (S_{i,j} - O_{i,j})^2}{N}\right) + 2k + \frac{2k(k+1)}{N-k-1} + N \cdot \ln(2\pi) + N \quad (27)$$

$$BIC_j = N \cdot \ln\left(\frac{\sum_{i=1}^N (S_{i,j} - O_{i,j})^2}{N}\right) + k \cdot \ln(N) + N \cdot \ln(2\pi) + N \quad (28)$$

where $RMSE_j$, $RRMSE_j$, r_j , R_j^2 , NSE_j , $Bias_j$, AIC_j and BIC_j are the metrics for the j th station; $O_{i,j}$ and $S_{i,j}$ respectively are observed and simulated values for the j th station at i th time step; N is the number of time steps (measurements), and k is the number of coefficients in the model; \bar{O}_j is the mean of observed values. The AIC_j and BIC_j metrics not only use the variance between observed and simulated values, but they also use the sample size (N) and the number of model parameters (k) to penalize the less parsimonious model(s). Calculated AIC and BIC increase linearly towards the non-optimal range by increasing the number of coefficients.

g. Testing LR equations

As presented in section 2.c, many formulations for longwave heat budget estimation exist. In this study, two methods for longwave calculation will be evaluated using ground-based measurements: (1) testing ERA5 data as a proxy instead of using DLI models and (2) estimating DLI using 20 forms of models for both clear and cloudy conditions (Table 2). Both cases are evaluated with ground-based observation for DLI using three installed sensors. For clear sky conditions, equations can be divided into two groups (Fig. 2): The first group is composed of formulations requiring the estimation of β , while the second group includes the formulations that do not require estimating β . The decision tree and selected models are as Fig. 2. The detailed parametrization is provided in Table 2.

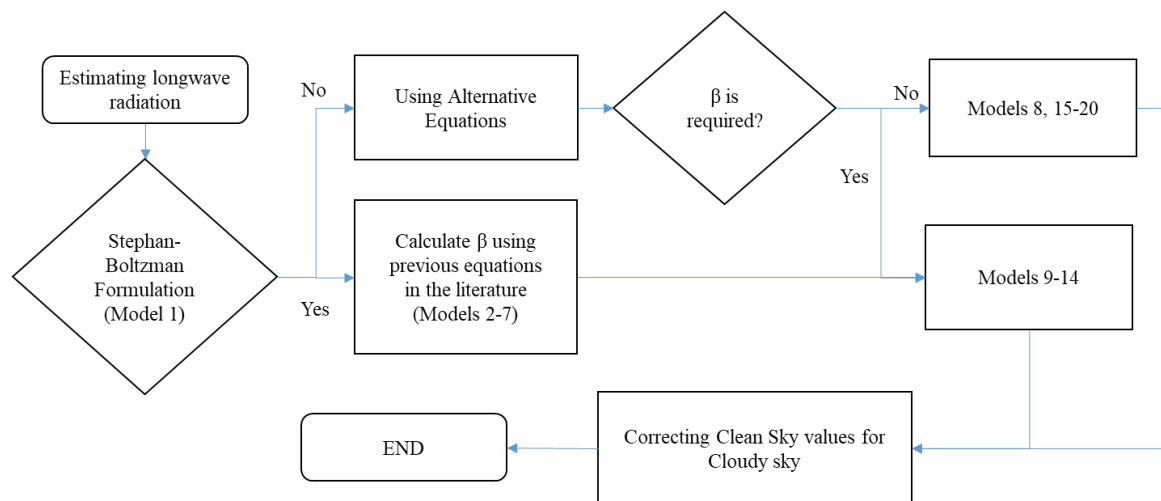


Fig. 2: Flowchart for calculation of DLI in different conditions using selected equations (Total number of options is 20)

Based on Fig. 2, 20 models (Table 2) will be tested using three net radiometers installed at the SLS, Kenny dam, and BVE stations. These net radiometers (Apogee) have four components: two pyranometers that measure incoming (upward-looking) and reflected (downward-looking) shortwave radiation and two pyrgeometer facing upward and downward for longwave radiations. All four radiation fluxes were recorded hourly for periods mentioned in Table 1.

The ERA5 variables were used without any correction as they were proposed as a reliable proxy for data-scarce regions or ungauged watersheds over Canada by Tarek et al. (2020). Also, the efficiency of the direct use of ERA5 products over the Nechako watershed was confirmed by Gatien et al. (2022) and Khorsandi et al. (2022).

Model No.	Based on Stephan-Boltzman	Equation for β	Equation
1	Yes	$\beta = 1$	$J_1 = (1 + u_1 B^{v_1}) \sigma T_{air}^4$
2	Yes	(Eq. 3)	$J_2 = (1 + u_2 B^{v_2}) [(0.74 + 0.0065 e_a) (1 + 0.17 B^2)] \sigma T_{air}^4$
3	Yes	(Eq. 4)	$J_3 = (1 + u_3 B^{v_3}) [(0.53 + 0.2055 e_a^{0.5}) (1 + 0.40 B)] \sigma T_{air}^4$
4	Yes	(Eq. 6)	$J_4 = (1 + u_4 B^{v_4}) (1 - a_4 \exp[b_4 (273 - T_{air})^2]) \sigma T_{air}^4$
5	Yes	(Eq. 7)	$J_5 = (1 + u_5 B^{v_5}) [a_5 (\frac{e_a}{T_{air}})^{b_5}] \sigma T_{air}^4$
6	Yes	(Eq. 8)	$J_6 = (1 + u_6 B^{v_6}) \langle a_6 [1 - \exp(-e_a \frac{T_{air}}{b_6})] \rangle \sigma T_{air}^4$
7	Yes	(Eq. 9)	$J_7 = (1 + u_7 B^{v_7}) (a_7 + b_7 e_a^{0.5}) \sigma T_{air}^4$
8	No	-	$J_8 = (1 + u_8 B^{v_8}) \{1 - 0.261 \exp(-0.000777 T_{air}^2) + \sigma (T_{air}^4 - [1 - 0.261 \exp(-0.000777 T_{air}^2)]) B^{1.4} \alpha_8\}$ $J_8 = (1 + u_8 B^{v_8}) \{1 - a_8 \exp(-b_8 T_{air}^2) + \sigma (T_{air}^4 - [1 - a_8 \exp(-b_8 T_{air}^2)]) B^{1.4} \alpha_8\}$
9	No	(Eq. 3)	$J_9 = (1 + u_9 B^{v_9}) [(0.74 + 0.0065 e_a) (1 + 0.17 B^2)] \sigma T_{air}^4 B^{-0.0227} \alpha_9$
10	No	(Eq. 4)	$J_{10} = (1 + u_{10} B^{v_{10}}) [(0.53 + 0.2055 e_a^{0.5}) (1 + 0.40 B)] \sigma T_{air}^4 B^{-0.0227} \alpha_{10}$
11	No	(Eq. 6)	$J_{11} = (1 + u_{11} B^{v_{11}}) (1 - a_{11} \exp[b_{11} (273 - T_{air})^2]) \sigma T_{air}^4 B^{-0.0227} \alpha_{11}$
12	No	(Eq. 7)	$J_{12} = (1 + u_{12} B^{v_{12}}) [a_{12} (\frac{e_a}{T_{air}})^{b_{12}}] \sigma T_{air}^4 B^{-0.0227} \alpha_{12}$
13	No	(Eq. 8)	$J_{13} = (1 + u_{13} B^{v_{13}}) \langle a_{13} [1 - \exp(-e_a \frac{T_{air}}{b_{13}})] \rangle \sigma T_{air}^4 B^{-0.0227} \alpha_{13}$
14	No	(Eq. 9)	$J_{14} = (1 + u_{14} B^{v_{14}}) (a_{14} + b_{14} e_a^{0.5}) \sigma T_{air}^4 B^{-0.0227} \alpha_{14}$
15	No	-	$J_{15} = (1 + u_{15} B^{v_{15}}) (5.16453 \times 10^{-13} [1 + (0.17 B^2)] T_{air}^6)$
16	No	-	$J_{16} = (1 + u_{16} B^{v_{16}}) (a_{16} + b_{16} T_{air} - c_{16} e_a - d_{16} \ln T_{air} - \frac{e_{16}}{T_{air}} + f_{16} \sqrt{e_a} + \frac{g_{16}}{e_a})$
17	No	-	$J_{17} = (1 + u_{17} B^{v_{17}}) (a_{17} T_{air}^2) \sigma T_{air}^4$
18	No	-	$J_{18} = (1 + u_{18} B^{v_{18}}) (1 - [1 + a_{18} (\frac{e_a}{T_{air}})] \exp\{-\{b_{18} + c_{18} [a_{18} (\frac{e_a}{T_{air}})]\}^{d_{18}}\}) \sigma T_{air}^4$
19	No	-	$J_{19} = (1 + u_{19} B^{v_{19}}) \langle a_{19} + b_{19} (\frac{T_{air}}{273.16})^6 + c_{19} \sqrt{\frac{e_a}{T_{air}}} \rangle$
20	No	-	$J_{20} = (1 + u_{20} B^{v_{20}}) \begin{cases} [a_{20} + b_{20} (e_a - 1.5)] \sigma T_{air}^4, & e_a \geq 1.5 \\ [a_{20} + c_{20} (e_a - 1.5)] \sigma T_{air}^4, & e_a < 1.5 \end{cases}$

Table 2. Formulation of the twenty DLI estimation models for this study (models are numbered from 1-20)

3. Results

The results presented here are a comparison of J_{air} obtained from the ERA5 reanalysis database together with the 20 models described in Table 2. Each equation shows the impact of cloud cover (B), vapor pressure (e_a) and air temperature (T) in estimating measured DLI.

a. Model calibration

Firstly, the calibration results for the SLS station are presented using the RMSE metric for different methods in Table 3. The calibrated coefficients for twenty models are shown in Table B1 in Appendix B. There is high variability between RMSEs obtained by various models from a minimum value $31.75 \frac{W}{m^2}$ (RRMSE = 11.7%, For ERA5 data) to maximum $267.3 \frac{W}{m^2}$ (RRMSE = 98.64%, For method 8). However, there is less variability between the remaining 19 models. This similarity of the results for the other 19 models is perhaps not surprising since the models are based on physical laws for radiation; however, the emissivity of the air is not similarly formulated. The ERA5 downward longwave radiation is superior to all models, which can be related to the fact that ERA5 products are the result of 3D modeling of radiation in the atmosphere using multiple layers of the atmosphere (Martens et al. 2020). Also, the $RMSE = 31.75 \frac{W}{m^2}$ is comparable to results by Long et al. (2021).

Secondly, each method's other efficiency metrics were calculated to provide multiple criteria for comparison (Table 3). The resulting RRMSEs, as a dimensionless metric but similar to RMSE, show that other than methods 3, 8, and 10, the remaining methods show RRMSE values of less than 20%, which offers relatively good performance. The RRMSE for ERA5 data as the benchmark is 11.7% for the SLS station as the calibration step. Since the RMSE and RRMSE for multiple methods are close, the other metric values were calculated and compared (Table 3). ERA5 shows the best performance NSE performance (NSE = 0.56), followed by methods 1, 5, and 19.

The NSE metric shows the determination power of the model compared to the mean of the values. The mean of values is a better estimate if a model has an NSE value less than zero. Therefore, this metric identifies the worst models, i.e., with $NSE \leq 0$, that should be ignored. It can be seen that models 3, 6, 8, 9, 10, 15, and 16 do not have enough determination power.

Other than ERA5 and models 1, 5, and 19, the remaining models (11, 12, 13, 14, 19, and 20) have similar NSE metrics (≈ 0.37). The R^2 values for these models show a similar range, too (≈ 0.39). As another metric, simple bias can be used. Models 1, 5, and 19 show the best Bias values. The only metrics that consider the complexity and performance of a model at the same time are AIC and BIC. These metrics identify the most parsimonious models with acceptable performance. Both AIC and BIC criteria show the minimum (best) value for ERA5, followed by models 1, 5, and 19, as the best options (Table 3). Models 11, 12, 13, 14, 19, and 20 again show similar good performances after the above candidates.

Model No.	RMSE	RRMSE	Correlation	R ²	NSE	Bias	AICc	BIC
ERA5	31.75	11.72	0.78	0.61	0.56	6.54	83384.97	83384.97
<i>1</i>	37.53 ³	13.85	0.62	0.39	0.38 ³	2.69 ²	85912.03 ³	85916.51 ³
2	45.44	16.77	0.63	0.39	0.10	27.03	88796.43	88800.90
3	74.81	27.61	0.62	0.38	-1.45	61.75	96318.15	96322.63
4	43.60	16.09	0.62	0.38	0.17	23.71	88178.66	88187.62
5	37.12 ¹	13.70	0.63	0.40	0.40 ¹	2.28 ¹	85751.82 ¹	85760.77 ¹
6	50.35	18.58	0.64 ³	0.40	-0.11	35.56	90347.76	90356.72
7	43.82	16.17	0.64 ²	0.41	0.16	26.02	88254.17	88263.12
8	267.30	98.64	0.06	0.00	-30.31	259.79	115531.67	115542.87
9	49.05	18.10	0.63	0.39	-0.05	33.55	89952.98	89959.69
10	58.92	21.75	0.61	0.38	-0.52	25.30	92718.82	92725.54
11	38.00	14.02	0.63	0.40	0.37	-4.70	86107.48	86118.68
12	38.19	14.09	0.63	0.39	0.36	-4.47	86179.74	86190.93
13	37.73	13.92	0.63	0.40	0.38	3.64 ³	85997.03	86008.23
14	38.27	14.12	0.63	0.39	0.36	-4.64	86212.38	86223.57
15	54.20	20.00	0.63	0.40	-0.29	40.47	91458.70	91465.41
16	48.44	17.88	0.60	0.36	-0.03	31.81	89777.20	89797.34
17	42.96	15.85	0.62	0.39	0.19	4.98	87952.12	87958.84
18	43.61	16.09	0.64 ¹	0.41	0.17	25.58	88186.16	88199.60
19	37.49 ²	13.83	0.62	0.39	0.38 ²	0.42	85901.68 ²	85912.88 ²
20	38.39	14.17	0.63	0.40	0.35	11.90	86258.84	86270.04

Table 3: Efficiency metrics for calibration step for ERA5 data and 20 calibrated irradiance equations compared with observed data at the SLS station. The best candidate is in bold based on each efficiency metric. The three alternatives after the best model are italicized, and the metrics are numbered

The scatter plots of estimations vs. observations for the best models are shown in Fig. 3.

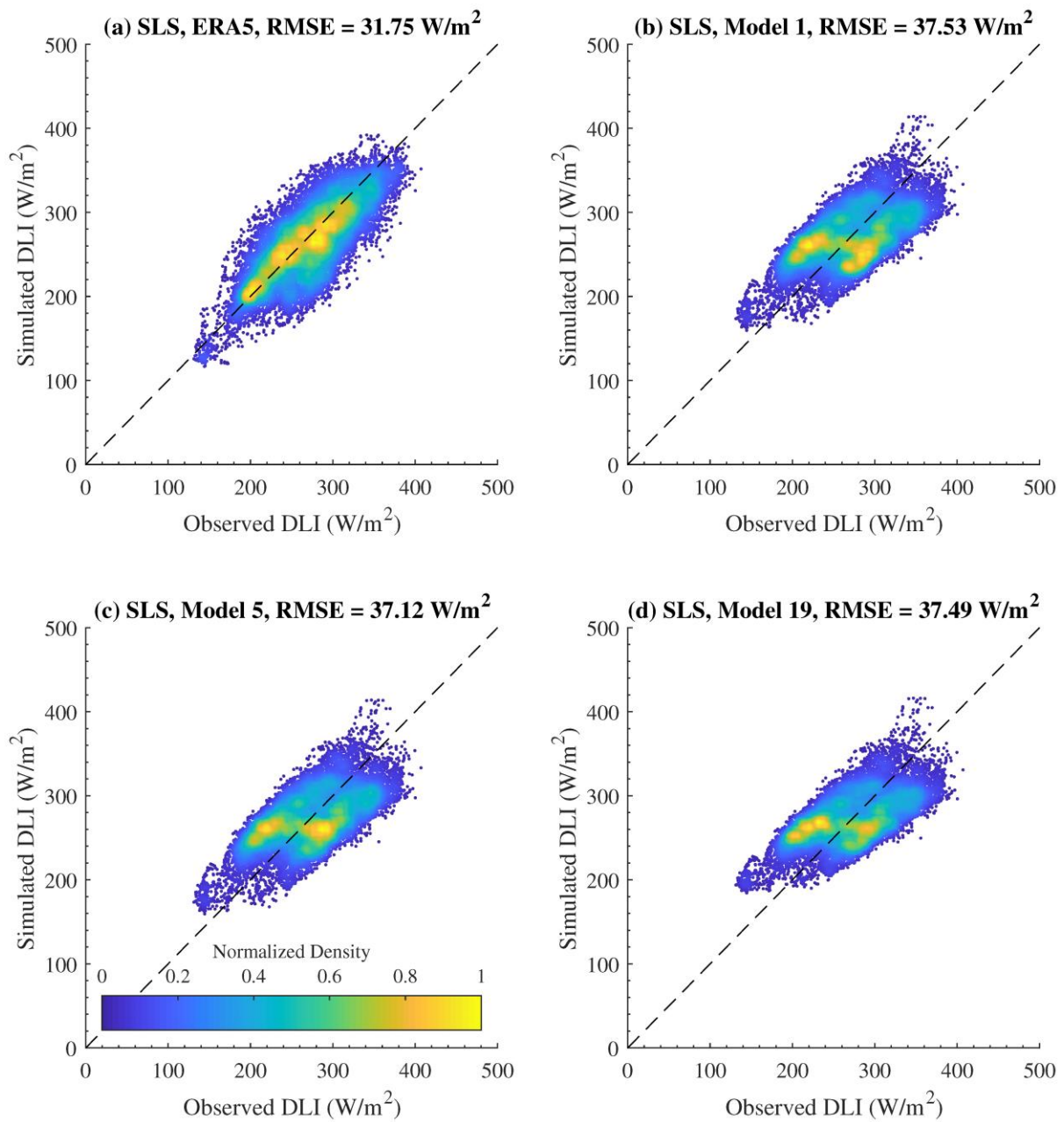


Fig. 3. Scatter plots for the best models for calibration at the SLS station. The models are: (a) for the ERA5 dataset, (b), (c), and (d) are the three selected alternatives, respectively, for models 1, 5, and 19 with their RMSE metrics

b. Model validations

With the calibrated parameters and equations from the calibration step on SLS, the validation results on the Kenny Dam and BVE stations are presented in Table 4 and Table 5.

Model No.	RMSE	RRMSE	Correlation	R ²	NSE	Bias	AICc	BIC
ERA5	34.62	12.77	0.75	0.56	0.47	8.92	84689.07	84689.07
<i>1</i>	38.38 ³	14.16	0.62	0.38	0.35 ¹	-0.81¹	86249.00 ³	86253.48 ³
2	46.34	17.10	0.61	0.37	0.06	25.78	89094.05	89098.53
3	76.35	28.18	0.60	0.36	-1.55	60.06	96624.38	96628.86
4	44.18	16.30	0.60	0.36	0.14	22.47	88375.85	88384.81
5	38.17 ²	14.09	0.62 ³	0.38	0.36 ²	1.06 ²	86171.38 ²	86180.34 ²
6	51.29	18.93	0.62	0.38	-0.15	34.71	90627.56	90636.52
7	44.33	16.36	0.62	0.38	0.14	25.54	88428.93	88437.89
8	272.28	100.48	0.07	0.01	-31.49	267.33	115810.33	115821.53
9	49.83	18.39	0.61	0.37	-0.09	32.59	90189.90	90196.62
10	62.46	23.05	0.60	0.36	-0.71	21.80	93598.31	93605.02
11	39.10	14.43	0.62 ²	0.38	0.33	-6.14	86538.30	86549.49
12	39.39	14.54	0.62	0.38	0.32	-6.07	86647.09	86658.29
13	38.93	14.37	0.62	0.38	0.34	2.15	86470.37	86481.57
14	39.50	14.58	0.62	0.38	0.32	-6.26	86689.37	86700.56
15	55.20	20.37	0.62	0.38	-0.34	39.49	91735.34	91742.06
16	48.58	17.93	0.59	0.35	-0.03	31.40	89819.27	89839.42
17	45.13	16.66	0.61	0.38	0.11	2.40	88696.60	88703.32
18	44.08	16.27	0.62 ¹	0.38	0.15	25.25	88346.09	88359.53
19	38.00 ¹	14.02	0.61	0.38	0.37 ¹	-1.13 ³	86106.17 ¹	86117.37 ¹
20	38.91	14.36	0.62	0.38	0.34	10.83	86461.58	86472.78

Table 4: Efficiency metrics as a validation step for ERA5 data and 20 DLI models compared with observed data at Kenny Dam station. The best candidate is in bold based on each efficiency metric. The three alternatives after the best model are italicized, and the metrics are numbered

Model No.	RMSE	RRMSE	Correlation	R ²	NSE	Bias	AICc	BIC
ERA5	47.33	15.90	0.77	0.59	0.57	0.01	134923.67	134923.67
<i>1</i>	<i>36.38³</i>	<i>12.22</i>	<i>0.89²</i>	<i>0.79</i>	<i>0.75³</i>	<i>4.22</i>	<i>128937.08³</i>	<i>128941.91³</i>
2	41.88	14.07	0.87	0.76	0.66	23.92	132146.54	132151.37
3	63.81	21.44	0.87	0.75	0.22	42.82	141730.38	141735.22
4	41.68	14.00	0.87	0.75	0.67	21.96	132039.46	132049.13
5	36.79	12.36	0.89	0.78	0.74	6.33	129196.28	129205.96
6	47.95	16.11	0.88	0.78	0.56	35.30	135230.91	135240.58
7	49.96	16.79	0.88	0.78	0.52	32.88	136165.58	136175.25
8	304.77	102.39	-0.01	0.00	-16.77	295.63	177329.85	177341.94
9	46.52	15.63	0.87	0.76	0.59	31.60	134536.96	134544.22
10	63.18	21.23	0.87	0.76	0.24	-4.01	141507.72	141514.97
11	36.98	12.42	0.89 ¹	0.79	0.74	0.38 ¹	129315.80	129327.89
<i>12</i>	<i>35.93²</i>	<i>12.07</i>	<i>0.89³</i>	<i>0.79</i>	<i>0.75²</i>	<i>-1.59²</i>	<i>128661.60²</i>	<i>128673.69²</i>
13	35.09	11.79	0.89	0.78	0.76	5.22	128125.82	128137.91
<i>14</i>	<i>35.82¹</i>	<i>12.03</i>	<i>0.89</i>	<i>0.78</i>	<i>0.75¹</i>	<i>-2.02³</i>	<i>128589.78¹</i>	<i>128601.87¹</i>
15	49.40	16.60	0.88	0.78	0.53	37.28	135906.37	135913.62
16	54.38	18.27	0.85	0.73	0.43	36.93	138105.11	138126.87
17	36.88	12.39	0.88	0.78	0.74	-4.84	129251.40	129258.66
18	52.69	17.70	0.89	0.78	0.47	34.65	137379.21	137393.72
19	38.45	12.92	0.88	0.78	0.72	5.11	130203.10	130215.19
20	40.37	13.56	0.89	0.78	0.69	16.76	131313.17	131325.26

Table 5: Efficiency metrics as a validation step for ERA5 data and 20 DLI models compared with observed data at BVE station. The best candidate is in bold based on each efficiency metric. The three alternatives after the best model are italicized, and the metrics are numbered

The results for the Kenny Dam station show very similar metrics and conclusions to the SLS station. Therefore, ERA5 and models 1, 5, and 19 provide the best estimates for these two stations belonging to the same watershed. The scatter plots for these models are presented in Fig. 4.

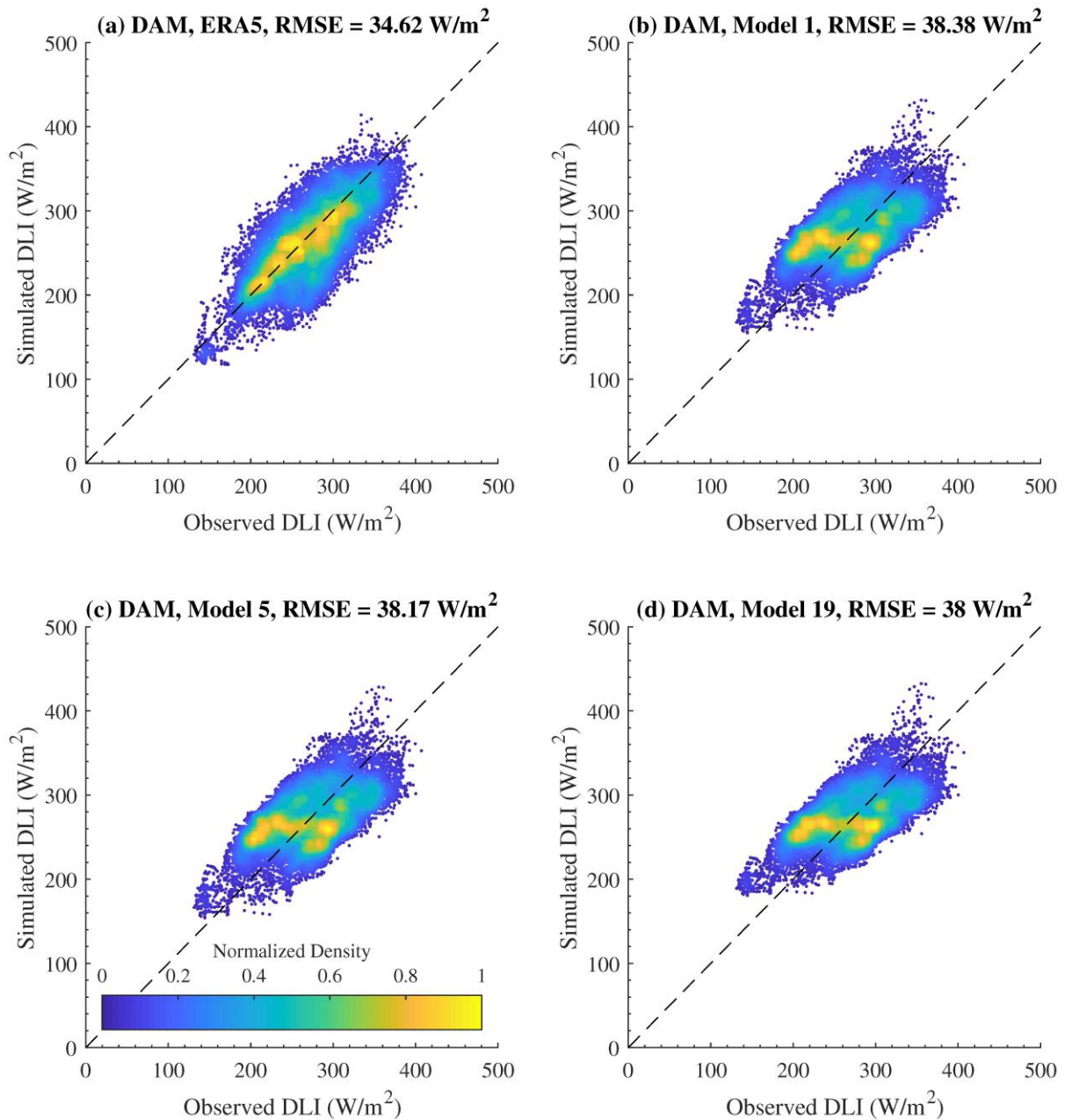


Fig. 4. Scatter plots for the best models for the validation step on Kenny Dam station. The models are: (a) for the ERA5 dataset, (b), (c), and (d) are the three selected alternatives, respectively, for models 1, 5, and 19 with their RMSE metrics

The validation results for the BVE station are somehow different. Model 13 shows the best performance for the majority of efficiency metrics in this station. The following alternative models are models 1, 12, and 14. A similar candidate for the two validation stations is model 1. Also, ERA5 does not provide the best metrics in any of the efficiency metrics. To facilitate

the interpretation of the results, scatter plots for these candidates are depicted in Fig. 5, together with models 5 and 19.

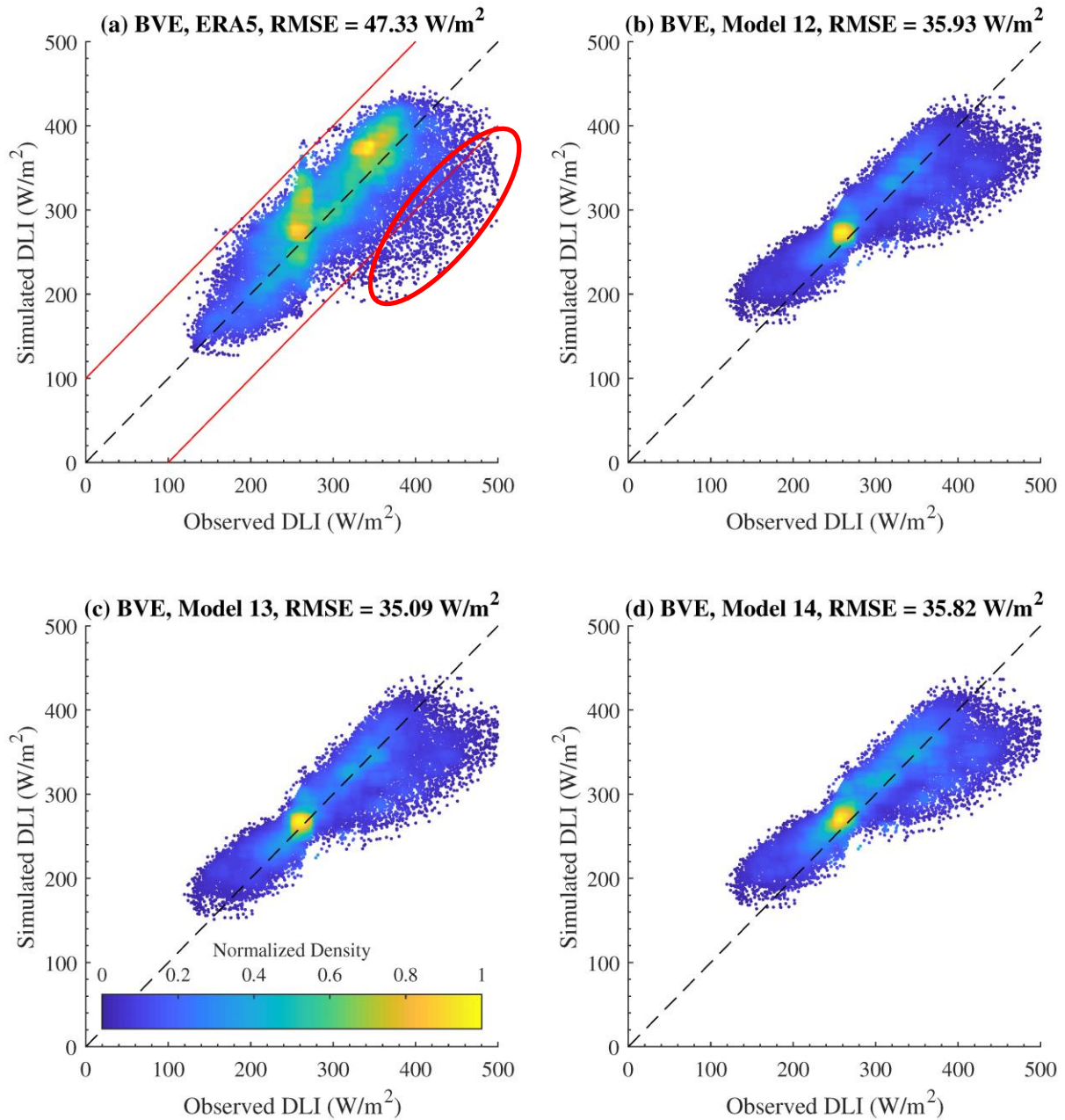


Fig. 5. Scatter plots for the best models for the validation step on the BVE station: (a) ERA5, (b) Model 12, (c) Model 13, and (d) Model 14. The best model is model 13, and the two selected alternatives are models 12 and 14, with their RMSE metrics. ERA5 results are also plotted for comparison. There is a systematic deviation among all the candidate models for a subset of data which is marked in red in panel (a)

Fig. 5 shows a systematic deviation among all the candidate models for a subset of data (marked in red in Fig. 5 for ERA5) for the BVE station compared with SLS or Kenny Dam stations. The magnitude of underestimation is $\geq 100 \text{ W/m}^2$. These larger measure values are due to the microclimate around the BVE station. These overestimated records cover the April-October period. This time of the year in Montreal, BVE station coincides with the growth of leaves on the trees and full canopy. To further analyze this fact, the whole validation step was repeated on BVE without using April-October records, and the resulted RMSE is 38.81 W/m^2 (RMSE for the whole period is 47.33 W/m^2 , based on Fig. 5a).

It is evident that the difference between a full canopy and bare leaf trees (BVE station is snow-covered during Nov-Mar) dramatically affects the DLI at the BVE station. The metrics for the partial time series in Fig. 6 are: $\text{RMSE} = 38.81 \text{ W/m}^2$, $\text{RRMSE} = 16.81\%$, $R^2 = 0.97$, and $\text{NSE} = 0.89$. The results show ERA5 data for the BVE station during Nov-Mar have comparable or better metrics than the SLS station. The high performance is associated with air temperatures $\leq 22^\circ\text{C}$ and all cloud conditions.

4. Discussion

Table B1 in Appendix B shows values of zero for the ν calibration parameter in the cloud correction factor $(1 + uB^\nu)$ for some models (Models 1, 2, 3, 8, 17, and 19). While u value is not equal to zero, it means the cloudiness correction factor to correct the longwave heat term is a constant, not changing with cloudiness. These values show the dominance of T_{air} compare to e_a in estimating DLI in agreement with Abramowitz et al. (2012).

Out of all formulations, model 8 has poor results and is not comparable with other models. Therefore, this formulation is not recommended for our study area. The other flawed model is number 17, which shows $a_{18} \approx 0$. This almost 0 value is faulty since it causes almost the same values for J_{air} no matter which meteorological variables are present. The efficiency metrics of this parametrization for calibration and validation are not among the best. Therefore this formulation is not recommended for the Nechako River watershed.

Not surprisingly, ERA5 data for DLI shows promising metrics among all models. This high level of performance is due to an improved scheme for radiation in the Integrated Forecasting System (IFS) for ECMWF (Hersbach et al. 2020; Hogan; Bozzo 2016; Urraca et al. 2018). However, for a single station, other models for DLI (formulations other than ERA5, 8, and 17) show comparable or even better performance than ERA5 data. This adequacy of the classic Stephan-Boltzmann equation for DLI agrees with Sugita; Brutsaert (1993). Further application

of these DLI models depends on the measured observations for humidity and cloud cover at the multiple layers of the atmosphere. Yao et al. (2019) suggest that the water clouds are generally overestimated in ERA5 and MERRA-2 for East Asia. However, our results for simulated DLI using total cloud cover don't show systematic biases for selected models (Fig. 3 and Fig. 4); however, some models show higher values for bias (Tables 3-5).

Further studies using cloud cover measurements at the atmosphere layers are needed to split the impact of data or model selection on DLI results. Although specific sensors are designed to measure the cloud cover parameters (www.atmos-meteo.com), to our knowledge, there are no measurements for such sensors in the Nechako watershed. Due to the lack of data for cloud cover-related variables, further studies are needed to validate reanalysis data for clouds in different layers of the atmosphere for Canada (Milewska 2004).

With a more careful look at the formulations and resulting parameters, we can see non-uniqueness among them, which means some of the equations are the same due to calibrated coefficients equal to zero. The original list can be shortened to 13 unique formulations (Numbered with roman numerals in Table C1 in Appendix C).

It is visible that the ERA5 dataset provides reliable estimates for DLI, directly usable for the lands without dense canopy. SLS and Kenny dam stations are open, unvegetated stations within a radius of 100 m of the installed sensors. However, the BVE station is surrounded by a thick canopy. It is visible that the local canopy effective distance (<100 m) is much less than the ERA5 grid distances (≈ 25 Km), so the ERA5 data can't be used to analyze the local canopy effects. Also, to compare a station's observed data with ERA5 data, the canopy effect should be eliminated as a pre-processing step. This canopy effect has two impacts at the BVE station:

First, there is a constant bias between observed DLI at the BVE station, compared to ERA5, and all the calibrated models. This effect is visible as a systematic bias (in this study and for BVE station ≈ 54 W/m²). This bias is not related to the leaf on the trees or the vapor pressure since it is present in all climate conditions over the year. Also, this bias is not associated with cloud effects since it is visible even in non-cloudy conditions. However, this longwave radiation is a local phenomenon possibly related to scattered DLI from non-living surfaces. Therefore, pre-processing was needed to eliminate this local effect from the observed data before comparing that with model results.

As the second impact, measurements at the BVE station show an overestimation in measured DLI values for the April-October period. This period is the growing season for

grasses and trees, and since the longwave absorption by snow is higher than the growing canopy, there is more DLI irradiance. These visible larger values for this specific period directly relate to DLI scattering, which is detected and observed by the sensor. Again, this canopy effect cannot be due to cloud cover, regardless of the amount of cloud cover and precisely for a specific period of the year.

At the same time, the results showed DLI from the ERA5 dataset does not need correction for elevation since the same product provides similar metrics for two validation stations in Eastern and Western Canada, with entirely different physiographies and elevations. The ECMWF global model includes the topography in the calculations for atmosphere-land interactions (Hersbach et al. 2020). The same reason is behind the reliable estimates for surface air temperature confirmed by Gatien et al. (2022) and Khorsandi et al. (2022) at the station scale and watershed scales in Nechako.

Out of the multiple models for DLI, three options (models 1, 5, and 19) show the most accurate estimations, which are our recommended options for future studies at the Nechako River watershed. This result agrees with Sugita and Brutsaert (1993), who mentioned that the Stephan-Boltzman formulation is accurate enough. The only problem is finding the correct formulation for β for cloudy conditions. Although using model 5 or 19 with four or five parameters marginally improved RRMSE compared to equation 1 (from 13.8% to 13.7 and 13.83% for calibration and from 14.16% to 14.09 and 14.02% for validation), it is at the price of adding two or three more parameters. It means cloud cover is the primary factor in controlling air emissivity, and vapor pressure (controlled by additional parameters) has a minor impact. The dominance of cloud cover in estimating β for the Nechako agrees with Huang et al. (2007) findings for outgoing longwave radiation and their results for the lower part of the atmosphere and Abramowitz et al. (2012) for DLI.

5. Conclusion

This study's main objective was to compare 20 models for DLI for the Nechako watershed in British Columbia, Canada. More precise models for DLI for this watershed can help the impact analysis of longwave heat budget on aquatic life. Calibration for each model at SLS's DLI was first performed, followed by validating those models on the Kenny Dam and BVE stations. Our results showed that the Stephan-Boltzman equation could provide reasonable estimates for DLI using the proper formulation to estimate β . Three formulations showed the best performance for both SLS and Kenny Dam, our proposed options for more hydrological

implementation at the Nechako watershed. Their superiority was shown using multiple metrics. Besides, the DLI downloaded data from the ERA5 reanalysis database provide the best results in terms of RMSE and RRMSE, which implies the direct use of ERA5 data instead of its calculation using a model. Our proposed options can be incorporated into hydrological models like CEQUEAU, which is of interest to decision-makers in the Nechako watershed. Since meteorological data have a significant local impact in this watershed and longwave radiation is one of the primary heat budget terms for water cooling during the summer, using more optimal options for DLI formulation can increase the model's prediction skill for water temperature modeling. This deterministic improved skill can also provide a better tool for climate change studies. Future studies are recommended to apply proposed models at the watershed scale using available deterministic hydrological models.

Acknowledgments

The authors would like to thank the anonymous reviewers for their insightful and constructive comments that helped us substantially improve the quality of our study. We thank Richard Loubier (Rio Tinto) and Michel Baraër (École de technologie supérieure) for providing longwave radiation data. This work was funded by the Canadian Natural Sciences and Engineering Research Council (NSERC) and Rio Tinto as part of a Collaborative Research and Development grant (Grant Number: CRDPJ 523640-18).

Data Availability Statement.

Due to its proprietary nature, supporting data cannot be publicly available. Further information about the data and conditions for access are available upon request from Rio Tinto via Email.

APPENDIX

Appendix A



Fig. A1: The location of three installed sensors (a) SLS at the Nechako watershed, (B) Kenny Dam at the Nechako watershed, and (c) BVE station at the BVE Sainte-Marthe watershed

Appendix B

Model No.	Calibrated Parameter Values									
	u	v	a	b	c	d	e	f	g	α
1	-0.17	0.00	-	-	-	-	-	-	-	-
2	-0.05	0.00	-	-	-	-	-	-	-	-
3	-0.39	0.00	-	-	-	-	-	-	-	-
4	0.18	4.00	0.26	0.00	-	-	-	-	-	-
5	0.07	4.00	0.82	0.00	-	-	-	-	-	-
6	0.23	2.05	1.00	2016.00	-	-	-	-	-	-
7	0.19	2.87	0.75	0.00	-	-	-	-	-	-
8	0.00	0.00	0.26	0.00	-	-	-	-	-	0.99
9	0.53	0.11	-	-	-	-	-	-	-	0.63
10	0.00	0.49	-	-	-	-	-	-	-	0.59
11	0.28	1.21	0.05	0.00	-	-	-	-	-	0.72
12	0.28	1.23	0.22	0.00	-	-	-	-	-	3.15
13	0.32	0.99	0.57	9173.20	-	-	-	-	-	1.79
14	0.28	1.25	0.64	0.00	-	-	-	-	-	1.06
15	0.07	0.22	-	-	-	-	-	-	-	1.06
16	0.22	1.62	1.01	0.75	4.97	0.00	0.00	0.00	0.00	-
17	0.59	0.00	0.00	-	-	-	-	-	-	-
18	0.19	2.75	5.47	3.28	4.84	0.30	-	-	-	-
19	0.70	0.00	68.37	81.30	36.86	-	-	-	-	-
20	0.18	6141.76	0.79	0.00	0.00	-	-	-	-	-

Table B1: Parameter values after the calibration step for the 20 calibrated DLI models in comparison with observed data at the SLS station

Appendix C

Model No.	Unique ID	Number of Parameters	Equation
1	I	1	$J = \alpha \sigma T_{air}^4$
4	II	3	$J = (1 + uB^v) \alpha \sigma T_{air}^4$
5			
7			
20			
11	III	4	$J = (1 + uB^v) \alpha \sigma T_{air}^4 B^{-0.0227}$
12			
14			
2	IV	1	$J = [(0.74 + 0.0065e_a)(1 + 0.17B^2)] \alpha \sigma T_{air}^4$
9	V	3	$J = (1 + uB^v) [(0.74 + 0.0065e_a)(1 + 0.17B^2)] \alpha \sigma T_{air}^4 B^{-0.0227}$
3	VI	1	$J = [(0.53 + 0.2055e_a^{0.5})(1 + 0.40B)] \alpha \sigma T_{air}^4$
10	VII	3	$J = (1 + uB^v) [(0.53 + 0.2055e_a^{0.5})(1 + 0.40B)] \alpha \sigma T_{air}^4 B^{-0.0227}$
6	VIII	4	$J = (1 + uB^v) \langle a [1 - \exp(-e_a \frac{T_{air}}{b})] \rangle \sigma T_{air}^4$
13	IX	5	$J = (1 + uB^v) [1 - \exp(-e_a \frac{T_{air}}{b})] \alpha \sigma T_{air}^4 B^{-0.0227}$
18	X	7	$J = (1 + uB^v) (1 - [1 + a (\frac{e_a}{T_{air}})] \exp \langle - \{ b + c [a (\frac{e_a}{T_{air}})] \} \rangle) \sigma T_{air}^4$
15	XI	2	$J = (1 + uB^v) \langle 5.16453 \times 10^{-13} [1 + (0.17B^2)] T_{air}^6 \rangle$
16	XII	5	$J = (1 + uB^v) (a + bT_{air} - ce_a)$
19	XIII	4	$J = \alpha \langle a + b (\frac{T_{air}}{273.16})^6 + c \sqrt{\langle \frac{e_a}{T_{air}} \rangle} \rangle$

Table C1: Final unique equation forms after simplifications, together with the number of parameters in each

REFERENCES

- Abramowitz, G., L. Pouyanné, and H. Ajami, 2012: On the information content of surface meteorology for downward atmospheric long-wave radiation synthesis. *Geophysical Research Letters*, **39**.
- Akaike, H., 1974: A new look at the statistical model identification. *IEEE Transactions on Automatic Control*, **19**, 716-723.
- Arsenault, R., A. Poulin, P. Côté, and F. Brissette, 2014: Comparison of stochastic optimization algorithms in hydrological model calibration. *Journal of Hydrologic Engineering*, **19**, 1374-1384.
- Barbaro, E., and Coauthors, 2010: Observational characterization of the downward atmospheric longwave radiation at the surface in the city of São Paulo. *Journal of Applied Meteorology and Climatology*, **49**, 2574-2590.
- Bárbaro, E. W., A. P. Oliveira, J. Soares, M. J. Ferreira, M. Z. Božnar, P. Mlakar, and J. F. Escobedo, 2009: Downward Atmospheric longwave radiation in the city of São Paulo. *AIP Conference Proceedings*, AIP, 447-450.
- Bernhardt, E. S., and Coauthors, 2022: Light and flow regimes regulate the metabolism of rivers. *Proceedings of the National Academy of Sciences*, **119**.
- Bolz, H., 1949: Die Abhängigkeit der infraroten Gegenstrahlung von der Bewölkung. *Z. Meteorol*, **3**.
- Brunt, D., 1932: Notes on radiation in the atmosphere. I. *Quarterly Journal of the Royal Meteorological Society*, **58**, 389-420.
- Brutsaert, W., 1975: On a derivable formula for long- wave radiation from clear skies. *Water resources research*, **11**, 742-744.
- Budyko, M. I., 1974: *Climate and life*. Academic Press, Inc.
- Choi, M., J. M. Jacobs, and W. P. Kustas, 2008: Assessment of clear and cloudy sky parameterizations for daily downwelling longwave radiation over different land surfaces in Florida, USA. *Geophysical research letters*, **35**.
- Crawford, T. M., and C. E. Duchon, 1999: An improved parameterization for estimating effective atmospheric emissivity for use in calculating daytime downwelling longwave radiation. *Journal of Applied Meteorology*, **38**, 474-480.
- Dilley, A., and D. O'brien, 1998: Estimating downward clear sky long- wave irradiance at the surface from screen temperature and precipitable water. *Quarterly Journal of the Royal Meteorological Society*, **124**, 1391-1401.
- Duarte, H. F., N. L. Dias, and S. R. Maggionto, 2006: Assessing daytime downward longwave radiation estimates for clear and cloudy skies in Southern Brazil. *Agricultural and Forest Meteorology*, **139**, 171-181.
- Fassnacht, S., 2001: Daytime long-wave radiation approximation for physical hydrological modelling of snowmelt: a case study of southwestern Ontario. *Soil-vegetation-atmosphere Transfer Schemes and Large-scale Hydrological Models: Proceedings of an International Symposium (Symposium S5) Held During the Sixth Scientific Assembly of the International Association of Hydrological Sciences (IAHS) at Maastricht, The Netherlands, from 18 to 27 July 2001*, IAHS, 279.
- Free, M., B. Sun, and H. L. Yoo, 2016: Comparison between Total Cloud Cover in Four Reanalysis Products and Cloud Measured by Visual Observations at U.S. Weather Stations. *Journal of Climate*, **29**, 2015-2021.
- Gatien, P., R. Arsenault, J.-L. Martel, and A. St-Hilaire, 2022: Using the ERA5 and ERA5-Land reanalysis datasets for river water temperature modelling in a data-scarce region.
- Gauch, M., and Coauthors, 2022: In Defense of Metrics: Metrics Sufficiently Encode Typical Human Preferences Regarding Hydrological Model Performance.

- Gupta, H. V., H. Kling, K. K. Yilmaz, and G. F. Martinez, 2009: Decomposition of the mean squared error and NSE performance criteria: Implications for improving hydrological modelling. *Journal of hydrology*, **377**, 80-91.
- Hansen, N., 2016: The CMA evolution strategy: A tutorial. *arXiv preprint arXiv:1604.00772*.
- Hansen, N., and A. Ostermeier, 1996: Adapting arbitrary normal mutation distributions in evolution strategies: The covariance matrix adaptation. *Proceedings of IEEE international conference on evolutionary computation*, Nagoya, Japan, IEEE, 312-317.
- Herrero, J., and M. Polo, 2012: Parameterization of atmospheric longwave emissivity in a mountainous site for all sky conditions. *Hydrology and earth system sciences*, **16**, 3139.
- Hersbach, H., and Coauthors, 2020: The ERA5 global reanalysis. *Quarterly Journal of the Royal Meteorological Society*, **146**, 1999-2049.
- Hogan, R. J., and A. Bozzo, 2016: *ECRAD: A new radiation scheme for the IFS*. European Centre for Medium-Range Weather Forecasts.
- Huang, Y., V. Ramaswamy, and B. Soden, 2007: An investigation of the sensitivity of the clear-sky outgoing longwave radiation to atmospheric temperature and water vapor. *Journal of Geophysical Research: Atmospheres*, **112**.
- Idso, S. B., and R. D. Jackson, 1969: Thermal radiation from the atmosphere. *Journal of Geophysical Research*, **74**, 5397-5403.
- Khorsandi, M., A. St-Hilaire, and R. Arsenault, 2022: Multisite calibration of a semi-distributed hydrologic and thermal model in a large Canadian watershed. *Hydrological Sciences Journal*.
- Koll, D. D., and T. W. Cronin, 2018: Earth's outgoing longwave radiation linear due to H₂O greenhouse effect. *Proceedings of the National Academy of Sciences*, **115**, 10293-10298.
- Krause, P., D. Boyle, and F. Bäse, 2005: Comparison of different efficiency criteria for hydrological model assessment. *Advances in geosciences*, **5**, 89-97.
- Lai, Y. G., and D. Mooney, 2009: On a two-dimensional temperature model: development and verification. *World Environmental and Water Resources Congress 2009: Great Rivers*, 1-14.
- Legates, D. R., and G. J. McCabe Jr, 1999: Evaluating the use of "goodness-of-fit" measures in hydrologic and hydroclimatic model validation. *Water resources research*, **35**, 233-241.
- Li, M., Y. Jiang, and C. F. M. Coimbra, 2017: On the determination of atmospheric longwave irradiance under all-sky conditions. *Solar Energy*, **144**, 40-48.
- Long, Z., L. Ding, J. Zhou, and T. Zhou, 2021: Toward the Estimation of All-Weather Daytime Downward Longwave Radiation over the Tibetan Plateau. *Atmosphere*, **12**, 1692.
- Martens, B., D. L. Schumacher, H. Wouters, J. Muñoz-Sabater, N. E. C. Verhoest, and D. G. Miralles, 2020: Evaluating the land-surface energy partitioning in ERA5. *Geosci. Model Dev.*, **13**, 4159-4181.
- McFarlane, V., and S. P. Clark, 2021: A detailed energy budget analysis of river supercooling and the importance of accurately quantifying net radiation to predict ice formation. *Hydrological Processes*, **35**, e14056.
- Milewska, E. J., 2004: Baseline cloudiness trends in Canada 1953–2002. *Atmosphere-Ocean*, **42**, 267-280.
- Miller, D. H., 1981: *Energy at the Surface of the Earth: An Introduction to the Energetics of Ecosystems*. Elsevier.
- Morcrette, J.-J., 2002: The surface downward longwave radiation in the ECMWF forecast system. *Journal of climate*, **15**, 1875-1892.
- Morin, G., and D. Couillard, 1990: Predicting river temperatures with a hydrological model. Chapter 5. *Encyclopedia of Fluid Mechanics: Surface and Groundwater Flow Phenomena*. Volk Gulf Publishing Company, Houston, Tex.

- Morin, G., T. J. Nzakimuena, and W. Sochanski, 1994: Predicting river water temperature using a conceptual model: the case of the Moisie River. *Canadian Journal of Civil Engineering*, **21**, 63-75.
- Niemelä, S., P. Räisänen, and H. Savijärvi, 2001: Comparison of surface radiative flux parameterizations: Part I: Longwave radiation. *Atmospheric research*, **58**, 1-18.
- Ouellet, V., Y. Secretan, A. St- Hilaire, and J. Morin, 2014: Water temperature modelling in a controlled environment: comparative study of heat budget equations. *Hydrological Processes*, **28**, 279-292.
- Prata, A., 1996: A new long- wave formula for estimating downward clear- sky radiation at the surface. *Quarterly Journal of the Royal Meteorological Society*, **122**, 1127-1151.
- Satterlund, D. R., 1979: An improved equation for estimating long-wave radiation from the atmosphere. *Water Resources Research*, **15**, 1649-1650.
- Schafer, S. A., 2017: What is the global impact of 3D cloud-radiation interactions?, University of Reading.
- Schwarz, G., 1978: Estimating the Dimension of a Model. *The Annals of Statistics*, **6**, 461-464, 464.
- Sellers, W. D., 1965: Physical climatology.
- Sicart, J. E., R. Hock, P. Ribstein, and J. P. Chazarin, 2010: Sky longwave radiation on tropical Andean glaciers: parameterization and sensitivity to atmospheric variables. *Journal of glaciology*, **56**, 854-860.
- Sugita, M., and W. Brutsaert, 1993: Cloud effect in the estimation of instantaneous downward longwave radiation. *Water Resources Research*, **29**, 599-605.
- Swinbank, W. C., 1963: Long- wave radiation from clear skies. *Quarterly Journal of the Royal Meteorological Society*, **89**, 339-348.
- Tang, W., J. Qin, K. Yang, F. Zhu, and X. Zhou, 2021: Does ERA5 outperform satellite products in estimating atmospheric downward longwave radiation at the surface? *Atmospheric Research*, **252**, 105453.
- Tarek, M., F. P. Brissette, and R. Arsenault, 2020: Evaluation of the ERA5 reanalysis as a potential reference dataset for hydrological modelling over North America. *Hydrol. Earth Syst. Sci.*, **24**, 2527-2544.
- Urraca, R., T. Huld, A. Gracia-Amillo, F. J. Martinez-de-Pison, F. Kaspar, and A. Sanz-Garcia, 2018: Evaluation of global horizontal irradiance estimates from ERA5 and COSMO-REA6 reanalyses using ground and satellite-based data. *Solar Energy*, **164**, 339-354.
- Voortman, B., R. Bartholomeus, S. Van der Zee, M. F. Bierkens, and J. P. M. Witte, 2015: Quantifying energy and water fluxes in dry dune ecosystems of the Netherlands. *Hydrology and Earth System Sciences*, **19**, 3787-3805.
- Yao, B., C. Liu, Y. Yin, Z. Liu, C. Shi, H. Iwabuchi, and F. Weng, 2019: Assessment of cloud properties from the reanalysis with satellite observations over East Asia. *Atmos. Meas. Tech. Discuss.*, 1-36.
- Yao, B., C. Liu, Y. Yin, Z. Liu, C. Shi, H. Iwabuchi, and F. Weng, 2020: Evaluation of cloud properties from reanalyses over East Asia with a radiance-based approach. *Atmos. Meas. Tech.*, **13**, 1033-1049.
- Zhou, Y. P., and R. D. Cess, 2000: Validation of longwave atmospheric radiation models using Atmospheric Radiation Measurement data. *Journal of Geophysical Research: Atmospheres*, **105**, 29703-29716.
- Zhou, Z., A. Lin, L. Wang, W. Qin, Y. Zhong, and L. He, 2020: Trends in downward surface shortwave radiation from multi- source data over China during 1984–2015. *International Journal of Climatology*, **40**, 3467-3485.